Computation of the Electromagnetic Fields and Induced Temperatures Within a Model of the Microwave-Irradiated Human Eye

ALLEN TAFLOVE AND MORRIS E. BRODWIN, SENIOR MEMBER, IEEE

Abstract—**The electromagnetic fields within a detailed model of the human eye and its surrounding bony orbit are calculated for two different frequencies of plane-wave irradiation: 750 MHz and 1.5 GHz. The computation is performed with a finite-difference algorithm for the time-dependent Maxwell's equations, carried out to the sinusoidal steady state. The heating potential, derived from the square of the electric field, is used to calculate the temperatures induced within the eyeball of the model. This computation is performed with the implicit alternating-direction (IAD) algorithm for the heat conduction equation. Using an order-of-magnitude estimate of the heat-sinking capacity of the retinal blood supply, it is determined that a hot spot exceeding 40.4°C occurs at the center of the model eyeball at an incident power level of 100 mW/cm² at 1.5 GHz.**

I. INTRODUCTION

AT PRESENT, little theoretical work has been done in solving for the temperature distribution induced by microwave radiation in complicated biological structures. The emphasis has been on experimental investigation. This has been brought about in part by the expensive and time-consuming numerical methods required to compute the electromagnetic fields within arbitrary dielectric scatterers. Indeed, inhomogeneous tissues of great complexity may require so much direct computer storage with well-known techniques that solution is virtually impossible.

The eye has been of special experimental interest because of evidence of microwave-induced cataracts in humans [1], [2]. Typical experiments involved the exposure of rabbits to high levels of microwave radiation over a short time interval and the observation of the induced lens opacification over a period of several weeks [3], [4]. The relevance of such studies was based upon the similarity of the anatomy of human and rabbit eyes. These experiments established time–power density threshold levels for cataract formation. Results indicated that the dose of microwave radiation required for lens injury is based upon average rather than peak power. The mechanism of microwave cataract formation is therefore most likely thermal [5]. A standard for human exposure, based upon such animal experimentation, has been published [6].

The use of animal experimentation to establish a human exposure standard for microwave radiation implies that the anatomy, physiology, and electromagnetic environment of the test animals can be related to that of humans. However, several elements of this relation remain unclear. In particular, the role of tissue structure in determining microwave absorption may be significant. We know that electromagnetic wave absorption in a lossy dielectric scatterer is a function of its shape and dimensions. It is quite possible that the eye–scatterer of man develops heating potential contours different in location and magnitude from those of the rabbit because of the dimensional and structural differences in tissue anatomy. This possibility must be explored if a more precise exposure standard for man is to be established. As Guy [7] has stated: "A high priority need in this area is a complete thermodynamic study of the eye under microwave exposure."

Direct experimentation with the living human eye using either cataractogenic exposures similar to those of [3], [4], or using implanted thermocouple techniques [8] is impermissible because of the tissue damage caused by the experimental procedure. Therefore, the microwave heating of the human eye must be studied using models of the actual organ. A theoretical approach would attempt to solve for the fields and temperatures using some analytical or numerical method. Such a model would postulate a near- or far-field irradiation, and simulate the tissue geometry and thermodynamics to the maximum possible extent. This is the approach taken in this paper.

Early theoretical work in the area of the biological effects of electromagnetic radiation centered on the irradiation of models of the entire human body [9]. However, because experimental work indicated that harmful local tissue temperature rises could occur, interest in partial body irradiation was stimulated. Cook proposed the solution of Maxwell's equations coupled with the heat conduction equation to solve the problem of local microwave heating [10]. He developed a theory for the heating of a tissue half-space composed of layers of skin, fat, and muscle, by incident plane waves. The temperature distribution predicted by the theory was verified in his reported experimental procedure. Shapiro *et al.* modeled the

Manuscript received March 21, 1975; revised May 20, 1975.

A. Taflove was with the Department of Electrical Engineering, Technological Institute, Northwestern University, Evanston, Ill. 60201. He is now with the Research Institute, Illinois Institute of Technology, Chicago, Ill. 60616.

M. E. Brodwin is with the Department of Electrical Engineering, Northwestern University, Evanston, Ill. 60201.

plane-wave irradiation of a cranial structure [11]. The absorbed power density within concentric spherical shells was calculated using an approach parallel to that of Stratton [12]. It was concluded that calculation of microwave heating using semi-infinite slab models is not accurate for tissue geometries where the ratio of the local radius of curvature to the wavelength is between 0.05 and 5. In effect, hot spots may develop deep within lossy, curved tissue scatterers of this size.

The work of Shapiro *et al.* may be scaled to model the eye as a lossy sphere in free space. Such a direct scaling suggests the presence of hot spots within the model eyeball because the important ratio parameter is of the order of one at microwave frequencies. Yet such a scaling is faulty in that it neglects the wave reflection effects of the tissues of the bony orbit which surround the eyeball. Unfortunately, any eye model that accounts for these effects is much more difficult to solve. Inclusion of the bony orbit eliminates the possibility of an analytic solution for the fields because the geometry is no longer amenable to classical separation-of-variables techniques. The improved eye model compels the use of some numerical method to solve for the electromagnetic fields.

Several computer techniques that appear relevant to this problem have appeared in the recent literature [13]–[16]. Each of these methods derives a set of linear equations for either field variables or for field expansion coefficients, and then solves the linear system with a suitable matrix inversion scheme. However, it seems that none of these methods has been used to solve the microwave irradiation of the eye. Inspection of the problems involved with each method indicates either difficulty in setting up the linear system, or in finding sufficient fast, direct-access computer storage to invert the matrix of the linear system.

In this paper, we report a calculation of the microwave fields within a detailed model of the human eye and its surrounding bony orbit. The fields are computed using the finite-difference, time-domain solution of Maxwell's equations discussed in a previous paper [17]. This technique has been found to yield first-order accurate solutions of the electromagnetic fields within arbitrary dielectric scatterers of the order of one wavelength in diameter, situated in free space or at the surface of a half-space. We also report a numerical solution of the heat conduction equation for the eyeball, using the computed microwave heating function as the source function. The heat equation is solved using the implicit alternating-direction (IAD) method [18], [19]. It is determined that a significant hot spot develops at the center of the eyeball of the model at an incident frequency of 1.5 GHz.

II. THE MICROWAVE SCATTERING MODEL

In this section we discuss the finite-difference lattice used for the eye and bony orbit microwave scattering problem. The lattice boundary planes and assumed coordinate axes are shown in Fig. 1. The field vector components are positioned at distinct half-interval points in the lattice, as shown in [17, fig. 1].

The lattice of Fig. 1 is a 19-by-39-by-19 array of unit-cell cubes, with a fixed unit-cell diameter δ equal to 1.25 mm. A space lattice point is denoted as $(i,j,k) = (i\delta,j\delta,k\delta)$, where i, j, and k are integers. The eye–scatterer is assumed to have even symmetry about lattice planes $x = 19\frac{1}{2}\delta$ and $z = 19\delta$. This symmetry allows large savings of computer storage by permitting the solution of the complete eye model with the programming of only one spatial quadrant of the model. δ is chosen large enough so that, using this symmetry, the lattice covers a 47.5-mm-by-48.75-mm-by-47.5-mm volume, which is sufficient to enclose most of the bony orbit. Yet δ is small enough to fulfill the accuracy requirement of 0.05 wavelength resolution in all tissue for frequencies up to about 1.5 GHz. The incident plane wave is assumed to have the field components E_z and H_x and propagate in the $+y$ direction. This wave is generated at lattice plane $y = 3\delta$ using a source condition. At planes $y = 0$, $y = 39\delta$, $x = \frac{1}{2}\delta$, and $z = 0$, the field components are determined using lattice-truncation conditions. The scatterer symmetry conditions, plane-wave source condition, and lattice-truncation conditions, are discussed in Section III of this paper.

The location of the lattice of Fig. 1 relative to the eyeball and to the front of the skull is shown schematically in Fig. 2, which depicts the location of planes $y = 0$ and $z = 19\delta$. The angles and dimensions of the skull cross section are based upon available cephalometric data [20]. In order to realize an evenly symmetric irradiation of the eye–scatterer, the incident wave is assumed to propagate in a direction parallel to the axis of one bony orbit. The selected orbital axis is assumed to be the intersection of the lattice symmetry planes $x = 19\frac{1}{2}\delta$ and $z = 19\delta$.

The skull surface of Fig. 2 is seen to be approximately parallel to the x axis of the lattice, within about 1 cm of the right edge of the orbit. Similarly, it may be shown that immediately above and below the rim of the orbit the skull surface is almost parallel to the z axis. To construct a model of the eye–scatterer with the assumed symmetry, we let the skull surface of the model extend to infinity parallel to the x–z plane. Thus the model orbit is an indentation centered at $(19\frac{1}{2},j,19)$ in an infinite, planar, bony layer. The space to the rear of this layer is assumed to contain only brain tissue. The major microwave reflection effects of the model result from the eyeball–orbit juxtaposition alone.

Using available anatomical data [20], [21], we sketch

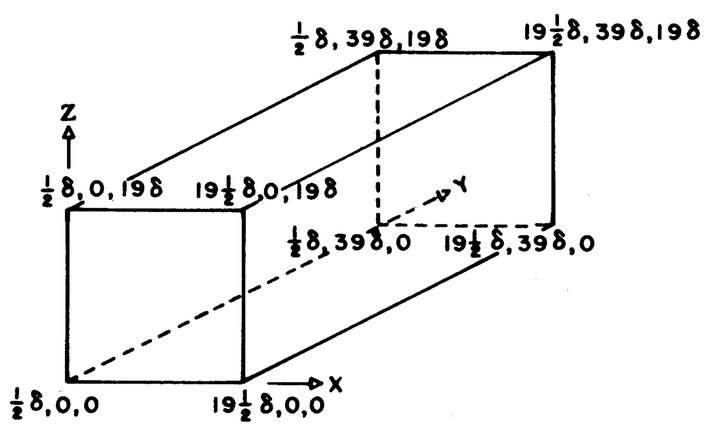

Fig. 1. Boundary planes of the finite-difference lattice used for the microwave scattering problem.

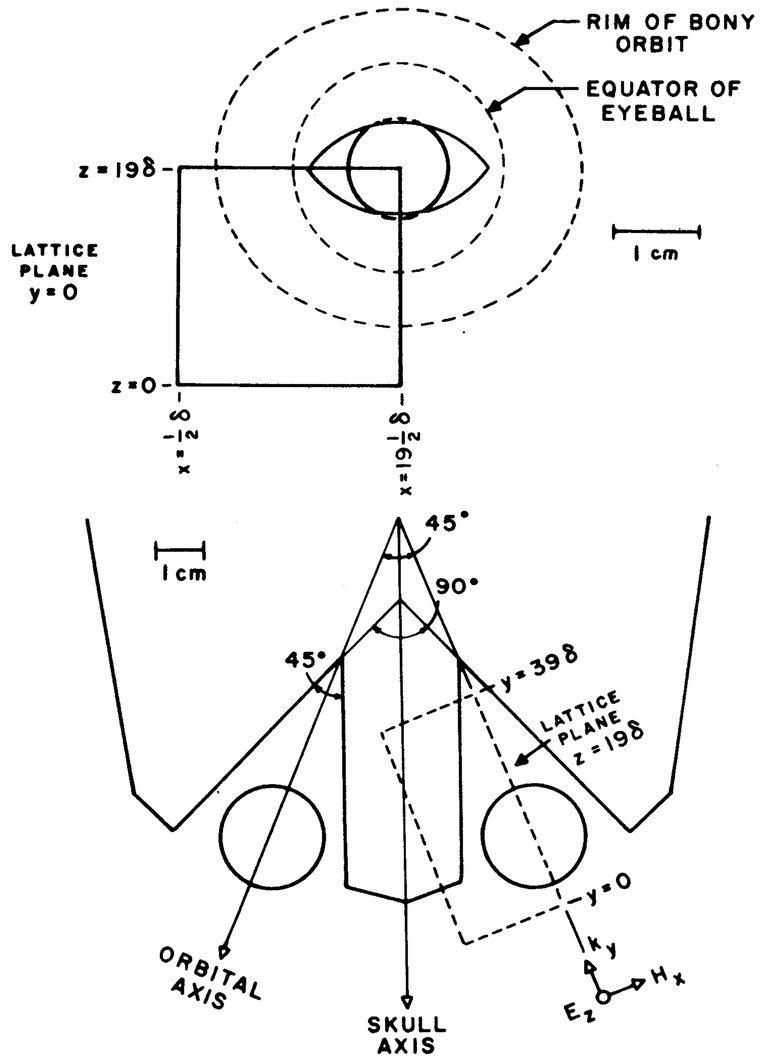

Fig. 2. Location of the lattice of Fig. 1 relative to the eyeball and the front of the human skull.

top and side views of the major tissues of the orbit in Fig. 3(a) and (b). The lattice of Fig. 1 contains an idealized, stepped-surface representation of the tissues of one quadrant of the orbit. This representation is depicted in Fig. 4(a) and (b) at the two lattice symmetry planes. Comparing Figs. 3 and 4 we see that the model eye simulates all rectus muscles associated with the eyeball. The symmetry assumptions, however, prevent simulation of the oblique muscles. In Fig. 4 no bone–fat interface is shown because of the similar dielectric parameters of these two tissues. Using published data on the composition of the eyeball media [21] and the electrical parameters of the other tissues found in the orbit [11], [22], the following values of ϵ and σ are assigned to each tissue.

Tissue Type	ϵ_r at: 750 MHz	1.5 GHz	σ (mhos/meter) at: 750 MHz	1.5 GHz
Skin, muscle, lens	52	49	1.54	1.77
Fat, bone	5.6	5.6	0.09	0.12
Eyeball humors	80	80	1.90	1.90
Brain, nerves	49	46	1.20	1.40

In constructing a model of the eye with the assumed symmetry, several simplifications of the actual tissue geometry are necessary. The symmetric model cannot take into account the curvature of the skull at the sides of the orbit, the sinus cavities of the skull, the existence of the oblique muscles, and the exact shape and thickness of the orbital wall. The accuracy of the model may be increased by omitting the assumed symmetry and using a lattice to cover the entire eye–scatterer. Further, the maximum frequency of irradiation may be increased by decreasing the lattice spacing. These elaborations are de-

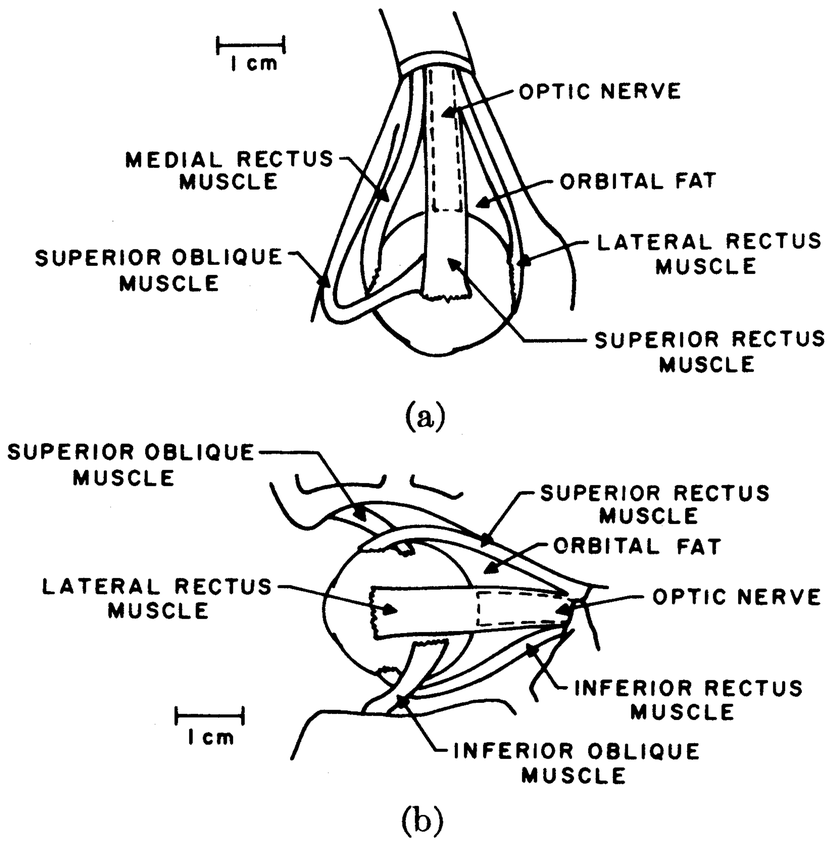

Fig. 3. The major tissues of the orbit. (a) Top view. (b) Side view.

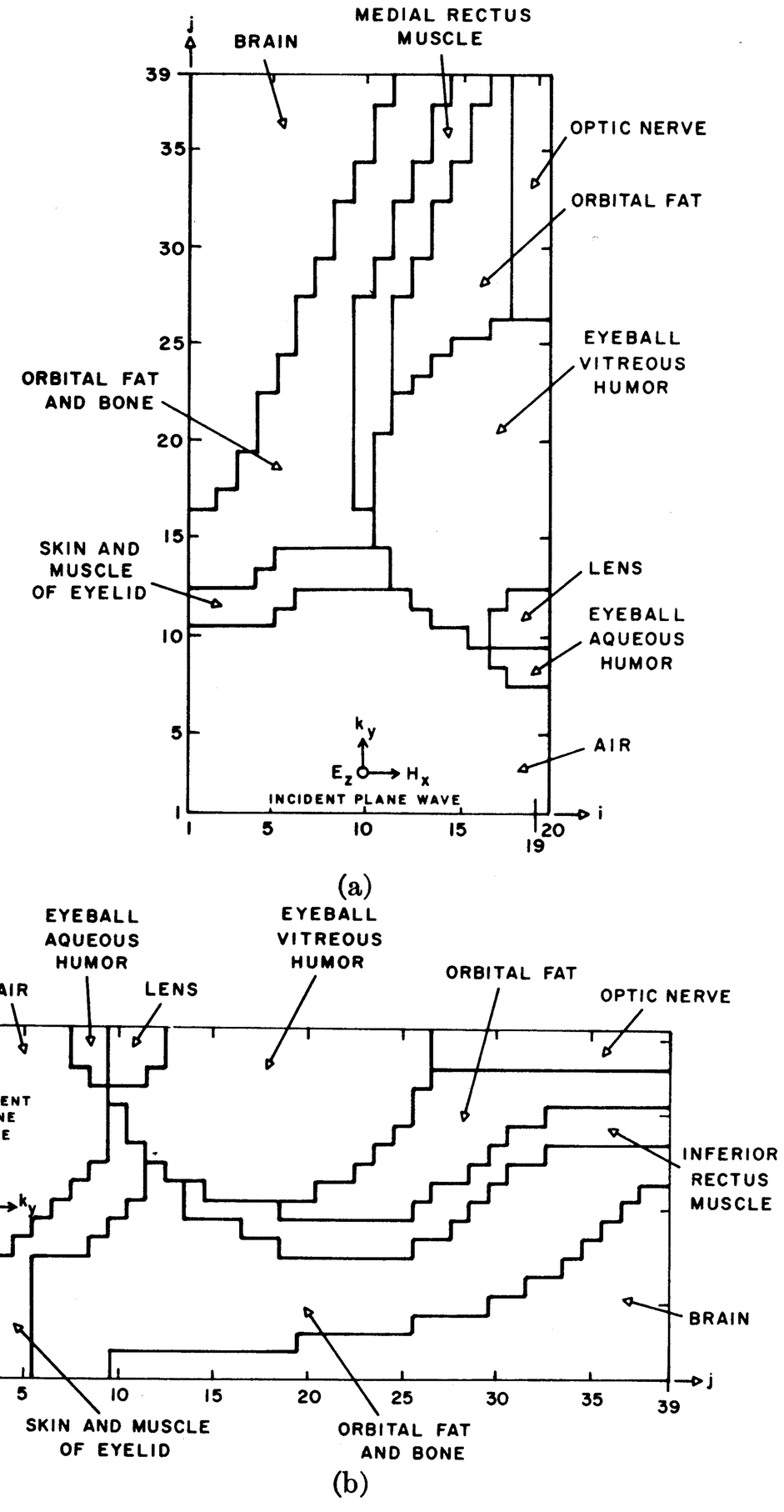

Fig. 4. Cross sections of the orbital tissues of the model at the lattice symmetry planes. (a) Plane $z = 19\delta$. (b) Plane $x = 19\frac{1}{2}\delta$.

pendent upon the acquisition of sufficient computer time on a machine with more fast storage capacity than the Northwestern University CDC 6400 which was used for the present research. However, the symmetric model simulates the basic geometry of the eye–scatterer, that of a water-like sphere encased in a low-loss dielectric cavity. This model should be accurate enough to locate and determine the magnitude of any high concentrations of microwave energy, with an acceptable level of uncertainty.

III. ELEMENTS OF THE MICROWAVE SCATTERING ALGORITHM[1]

In this section we discuss the modifications of the algorithm of [17] necessary for the present research. These modifications include a time-stepping algorithm with fewer multiplications, simpler symmetry conditions, adaptive lattice-truncation conditions, and increased stability considerations. In the discussion, any function of space and time is denoted as $F^n(i,j,k) = F(i\delta,j\delta,k\delta,n\delta t)$.

Assuming that the quantity $\delta t/\mu(i,j,k)\delta$ is constant for all (i,j,k) of the lattice, the algorithm of (6a)–(6f) of [17] requires nine multiplications per unit cell per time step. The number of required multiplications can be reduced to six and the algorithm considerably simplified in the following manner. We define the constants

$$R = \delta t/\epsilon_0 \tag{1a}$$

$$R_a = \delta t^2/(\delta^2\mu_0\epsilon_0) \tag{1b}$$

$$R_b = \delta t/\mu_0\delta \tag{1c}$$

$$C_a(m) = 1.0 - R\sigma(m)/\epsilon_r(m) \tag{1d}$$

$$C_b(m) = R_a/\epsilon_r(m) \tag{1e}$$

where m is a tissue-type integer from 1 to 5 assigned in the following way: 1, air; 2, skin, muscle, lens tissue; 3, fat, bone tissue; 4, eyeball humors; 5, brain, nerve tissue. We also define the proportional electric-field vector

$$\tilde{\boldsymbol{E}} = R_b\boldsymbol{E}. \tag{2}$$

Using the definitions of (1a)–(1e) and (2), we rewrite [17, eq. (6a)–(6c)] in a manner similar to the following:

$$\begin{aligned} H_x^{n+1/2}(i,j+\tfrac{1}{2},k+\tfrac{1}{2}) = {} & H_x^{n-1/2}(i,j+\tfrac{1}{2},k+\tfrac{1}{2}) \\ & + \tilde{E}_y^n(i,j+\tfrac{1}{2},k+1) \\ & - \tilde{E}_y^n(i,j+\tfrac{1}{2},k) \\ & + \tilde{E}_z^n(i,j,k+\tfrac{1}{2}) \\ & - \tilde{E}_z^n(i,j+1,k+\tfrac{1}{2}). \end{aligned} \tag{3}$$

This modification eliminates the three multiplications previously needed in the $\boldsymbol{H}$ part of the algorithm. Further, we rewrite [17, eq. (6d)–(6f)] in a manner similar to the following:

$$m = \text{MEDIA}(i+\tfrac{1}{2},j,k) \tag{4a}$$

$$\begin{aligned} \tilde{E}_x^{n+1}(i+\tfrac{1}{2},j,k) = {} & C_a(m)\tilde{E}_x^n(i+\tfrac{1}{2},j,k) \\ & + C_b(m)[H_z^{n+1/2}(i+\tfrac{1}{2},j+\tfrac{1}{2},k) \\ & - H_z^{n+1/2}(i+\tfrac{1}{2},j-\tfrac{1}{2},k) \\ & + H_y^{n+1/2}(i+\tfrac{1}{2},j,k-\tfrac{1}{2}) \\ & - H_y^{n+1/2}(i+\tfrac{1}{2},j,k+\tfrac{1}{2})]. \end{aligned} \tag{4b}$$

This modification eliminates the need for computer storage of separate ϵ and σ lattices. Now, only a MEDIA lattice, which specifies the tissue type at each lattice point, need be stored. In addition, the ϵ_r and σ of each tissue can now be changed without having to repunch a large data card deck. Such a change involves only the recalculation of the five values of $C_a(m)$ and the five values of $C_b(m)$. Finally, we rewrite [17, eq. (10)] as

$$\tilde{E}_z^n(i,3,k+\tfrac{1}{2}) \leftarrow 1000R_b \sin(2\pi \text{ fn } \delta t) + \tilde{E}_z^n(i,3,k+\tfrac{1}{2}). \tag{5}$$

This modification is needed to provide a plane-wave source condition at lattice plane $y = 3\delta$ that agrees with the definition of $\tilde{\boldsymbol{E}}$.

Symmetry condition [17, eq. (12)] requires extension of the lattice 0.5δ beyond the plane of symmetry. A set of conditions useful for the assumed even symmetry of the eye–scatterer, and requiring no lattice points beyond the symmetry planes, is given as

$$H_y^n(19\tfrac{1}{2},j,k+\tfrac{1}{2}) = H_z^n(19\tfrac{1}{2},j+\tfrac{1}{2},k) = 0 \tag{6a}$$

$$\tilde{E}_x^n(i+\tfrac{1}{2},j,19) = \tilde{E}_y^n(i,j+\tfrac{1}{2},19) = 0. \tag{6b}$$

We next consider a set of simple, approximate lattice-truncation conditions analogous to [17, eq. [9a)–(9d)]. From the basic time-step relation of this algorithm

$$2c\delta t = \delta \tag{7}$$

it is seen that a wave requires two time steps to propagate across a single unit cell, in air. We define the integer constant

$$l(m) = 2\lambda(1)/\lambda(m), \qquad \lambda(m)\text{: wavelength in tissue-type } m \tag{8}$$

as the number of time steps required for a wave to propagate across a single unit cell, in tissue-type m. We also define the stored field vectors

$$\hat{\tilde{\boldsymbol{E}}}(i,j,k) = \tilde{\boldsymbol{E}}^{n-l(\text{MEDIA}(i,j,k)}(i,j,k) \tag{9a}$$

$$\hat{\boldsymbol{H}}(i,j,k) = \boldsymbol{H}^{n-l(\text{MEDIA}(i,j,k)}(i,j,k). \tag{9b}$$

Then the truncation condition for lattice plane $x = \frac{1}{2}\delta$ is given by

$$\begin{aligned} H_y^n(\tfrac{1}{2},j,k+\tfrac{1}{2}) = {} & [\hat{H}_y(\tfrac{3}{2},j,k-\tfrac{1}{2}) + \hat{H}_y(\tfrac{3}{2},j,k+\tfrac{1}{2}) \\ & + \hat{H}_y(\tfrac{3}{2},j,k+\tfrac{3}{2})]/3 \end{aligned} \tag{10a}$$

[1] The listing of the 362 card Fortran IV source deck is available from the authors.

$$H_z{}^n(\tfrac{1}{2},j+\tfrac{1}{2},k) = [\hat{H}_z(\tfrac{3}{2},j+\tfrac{1}{2},k-1) + \hat{H}_z(\tfrac{3}{2},j+\tfrac{1}{2},k) + \hat{H}_z(\tfrac{3}{2},j+\tfrac{1}{2},k+1)]/3. \quad (10b)$$

For plane $y = 0$

$$\tilde{E}_x{}^n(i+\tfrac{1}{2},0,k) = \tilde{E}_x{}^{n-2}(i+\tfrac{1}{2},1,k) \quad (10c)$$

$$\tilde{E}_z{}^n(i,0,k+\tfrac{1}{2}) = \tilde{E}_z{}^{n-2}(i,1,k+\tfrac{1}{2}). \quad (10d)$$

For plane $y = 39\delta$

$$\tilde{E}_x{}^n(i+\tfrac{1}{2},39,k) = \hat{\tilde{E}}_x(i+\tfrac{1}{2},38,k) \quad (10e)$$

$$\tilde{E}_z{}^n(i,39,k+\tfrac{1}{2}) = \hat{\tilde{E}}_z(i,38,k+\tfrac{1}{2}). \quad (10f)$$

For plane $z = 0$

$$\tilde{E}_x{}^n(i+\tfrac{1}{2},j,0) = [\hat{\tilde{E}}_x(i-\tfrac{1}{2},j,1) + \hat{\tilde{E}}_x(i+\tfrac{1}{2},j,1) + \hat{\tilde{E}}_x(i+\tfrac{3}{2},j,1)]/3 \quad (10g)$$

$$\tilde{E}_y{}^n(i,j+\tfrac{1}{2},0) = [\hat{\tilde{E}}_y(i-1,j+\tfrac{1}{2},1) + \hat{\tilde{E}}_y(i,j+\tfrac{1}{2},1) + \hat{\tilde{E}}_y(i+1,j+\tfrac{1}{2},1)]/3. \quad (10h)$$

To illustrate the use of the lattice-truncation conditions, we consider the programming implementation of (10e) at point $(i+\frac{1}{2},39,k)$. The values $\tilde{E}_x{}^{n-1}(i+\frac{1}{2},38,k)$, $\hat{\tilde{E}}_x{}^{n-2}(i+\frac{1}{2},38,k),\cdots,\hat{\tilde{E}}_x(i+\frac{1}{2},38,k),\tilde{E}_x{}^n(i+\frac{1}{2},39,k)$ are stored in an array which is manipulated like a shift register, with one shift for each time step. This simulates the propagation delay of a scattered wave between the lattice planes $y = 38\delta$ and $y = 39\delta$. The propagation delays of several types of tissue can be simulated by providing a sufficiently large register to account for the maximum delay case, and by performing the shifting operation through only $l(\text{MEDIA}(i+\frac{1}{2},38,k)) + 1$ words of the array. In this way the truncation condition can be made to adapt to the type of tissue at each lattice-truncation plane.

We now consider the problem of the stability of the overall algorithm. A comparison of the value of δt of (7) with the maximum value of δt allowed by stability condition [17, eq. (14b)]

$$\delta t = \frac{\delta}{2c} < \frac{\delta}{c(3)^{1/2}} \quad (11)$$

indicates that the time-stepping algorithm should be absolutely stable. However, the inclusion of the lattice-truncation conditions perturbs the basic algorithm to the extent that this is not correct. Equations (10a)–(10h) have been found to induce a slowly growing instability. No simple reformulation of the lattice truncations has yet been found that eliminates this problem while still holding wave reflections at the truncations to an acceptable level. The growth of the instability has been found to be greatly slowed by increasing the size of the lattice, or by increasing the losses of the dielectric media of the lattice. The modeling of the irradiation of the eye–scatterer is made possible by assuming a small value of σ for the air in front of the eye. At 750 MHz, $\sigma(1) = 0.04$ mho/m; at 1.5 GHz, $\sigma(1) = 0.025$ mho/m. These values of conductivity are chosen small enough so that the incident fields are reduced less than 10 percent in propagating from the wave source at $y = 3\delta$ to the surface of the scatterer; yet these values are large enough to suppress the instability for more than 600 time steps of the algorithm. This is sufficient time for the fields to reach the sinusoidal steady state.

IV. RESULTS OF THE MICROWAVE SCATTERING PROGRAMS

In this section we compare the results of the microwave scattering programs for two different frequencies of irradiation, 750 MHz and 1.5 GHz. The storage and execution time requirements of each program are noted. Next, the computed results are presented as contour maps of the normalized heating potential Q_n at the two symmetry planes of the lattice. Last, the accuracy of the locations and magnitudes of the contours of Q_n is estimated.

Each run of the microwave scattering program required about 16 000 words of central memory and 213 280 words of extended core storage for compilation. A high-optimization Fortran compiler was used to minimize the execution time of each run. The 750-MHz program was run 640 time steps (with $\delta t = \delta/2c = 2.083$ ps), or exactly one cycle of the incident wave. Over the last half-cycle of the incident wave, or 320 time steps, the program determined the envelope of the electric field at each unit cell of the lattice. A total of 2300-s central processor time was required to execute this run. The 1.5-GHz program was run 600 time steps (with $\delta t = 2.083$ ps). This reduction of 40 time steps from the previous run was necessary to avoid the onset of instability which was hastened by the use of a smaller value of $\sigma(1)$ for this run. The envelope of the electric field was determined over the last half-cycle of the incident wave, or 160 time steps. A total of 2100 s was required for program execution.

Fig. 5(a) and (b) gives contour maps of the computed, normalized heating potential

$$Q_n(i,j,k) = \tfrac{1}{2}\sigma(i,j,k)\,|\,\boldsymbol{E}(i,j,k)\,|^2/E_{\text{inc}}{}^2$$

at lattice symmetry plane $z = 19\delta$, for incident frequencies of 750 MHz and 1.5 GHz, respectively. Fig. 6(a) and (b) are the corresponding maps at symmetry plane $x = 19\frac{1}{2}\delta$. In all of the maps the dashed lines indicate the boundaries of the tissues.

Within the model eyeball, the heating potential due to irradiation at 750 MHz peaks at the muscle interface at the front of the eye and gradually decreases with depth. Some peaking is noted at the muscle interface directly below the eye. Assuming an incident power level P_{inc} of 100 mW/cm^2, the total power dissipated within the model eye is 0.13 W. The average density of absorbed power for this condition is 0.022 W/cm^3 (assuming a model eyeball volume of 5.9 cm^3). The peak absorbed power density at the front of the eye is 0.16 W/cm^3, a level 7.3 times the average. For comparison, we note the measured data obtained by Guy *et al.* [8] for the rabbit eye irradiated at 915 MHz at the level P_{inc}. Here, absorption was almost

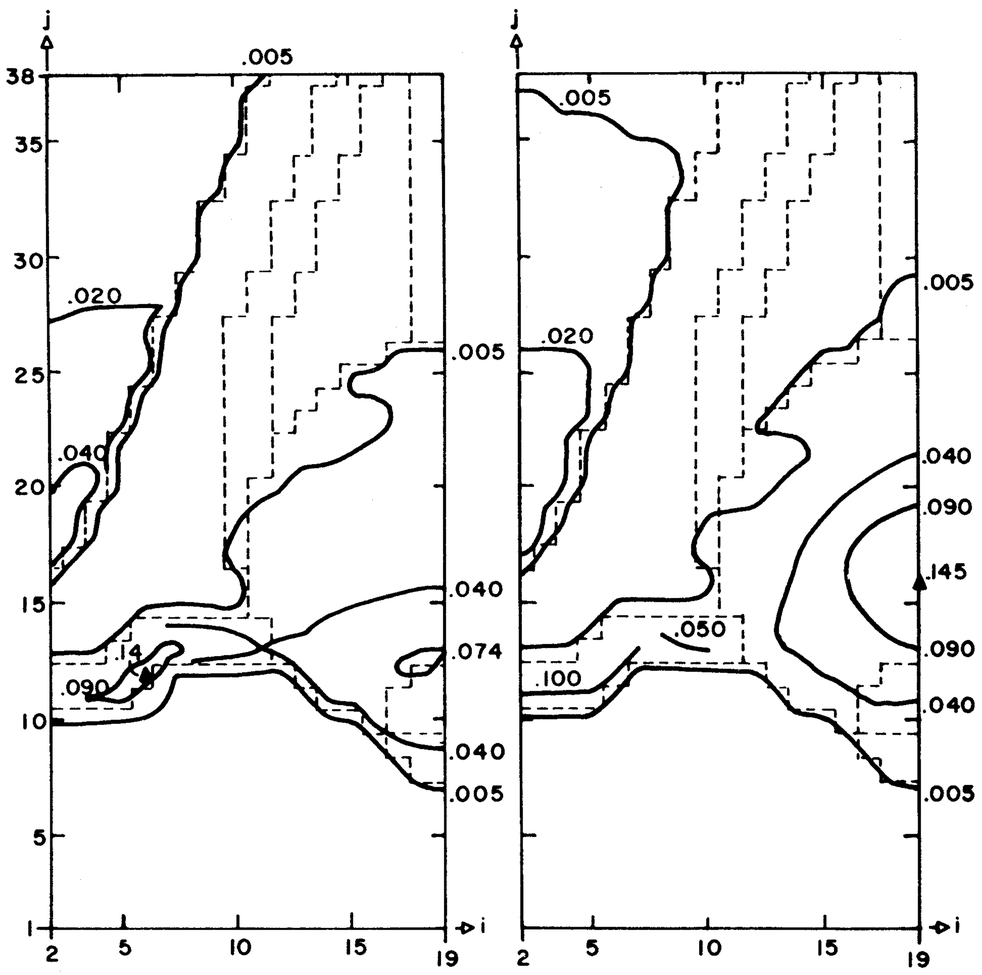

(a) (b)

Fig. 5. Maps of the computed, normalized heating potential Q_n at lattice symmetry plane $z = 19\delta$. (a) Incident frequency = 750 MHz. (b) Incident frequency = 1.5 GHz.

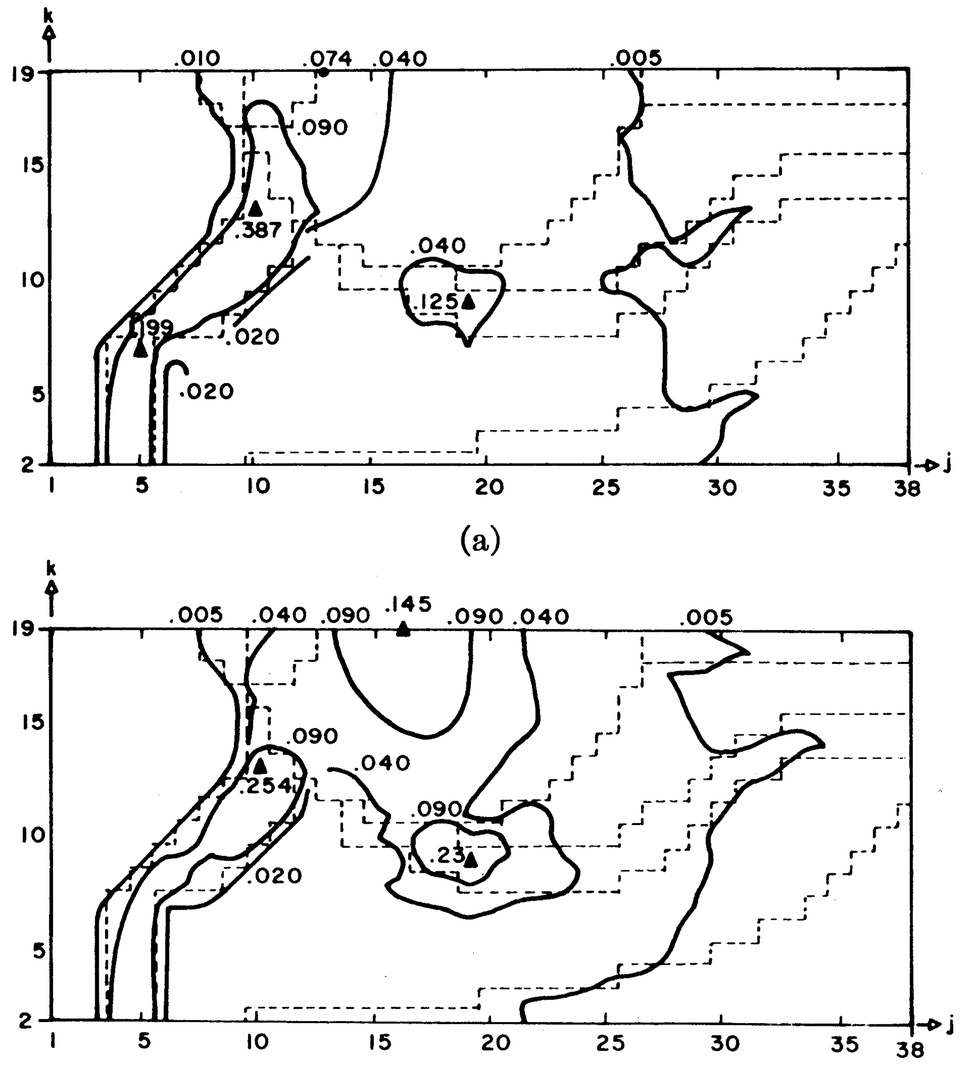

(a)

(b)

Fig. 6. Maps of the computed, normalized heating potential Q_n at lattice symmetry plane $x = 19\frac{1}{2}\delta$. (a) Incident frequency = 750 MHz. (b) Incident frequency = 1.5 GHz.

constant within the eyeball at a density of 0.024 W/cm³, but peaked to 0.036 W/cm³, 1 cm behind the orbit in the brain.

The heating potential due to 1.5-GHz irradiation shows a pronounced peak near the center of the model eyeball. The potential also peaks strongly at the muscle interfaces below and in front of the eye. Assuming $P_{inc} = 100$ mW/cm², the total power dissipated within the model eye is 0.19 W. The average absorbed power density for this condition is 0.033 W/cm³. The peak absorbed power density at the center of the eyeball is 0.11 W/cm³, a level 3.3 times the average. For comparison, we again note the data of Guy *et al.*, but consider the results for the rabbit irradiated at 2.45 GHz at the level P_{inc}. Here a distinct peak was observed in the vitreous body near the retina with a density of 0.092 W/cm³.

The frequency-dependent position of the heating potential peak reported in this paper and observed by Guy *et al.* in the rabbit might be explained on the basis of distinct resonances of the eye–scatterer and the head as a whole. At the lower microwave frequency, the dimensions of the eye–orbit combination are too small to support a wave concentration effect. Any peaking is probably due to a resonance of the whole head and should therefore occur behind the orbit in the brain as Guy *et al.* observed. However, at the higher microwave frequency, the eye–scatterer can support a resonant behavior independent of possible concentration effects of the whole head. Therefore, heating potential peaks are expected within the tissues of the orbit above 1.5 GHz.

Any estimate of the accuracy of the microwave scattering model of the eye must take into account both the accuracy of the tissue model and the accuracy of the computer algorithm. The simplifications of the tissue model have been discussed in Section II of this paper. Assuming that this model conforms to the physical reality, we estimate that the algorithm locates heating potential peaks and contours with a maximum error of $\pm 2\delta$, or about ± 10 percent of the diameter of the eyeball. The uncertainty of the magnitudes of the heating potential peaks is estimated as ± 10 percent. These estimates are based upon prior runs of the algorithm for geometries solvable by analytic methods. The main sources of error have been found to be the stepped-surface approximation of the scatterer and the residual wave reflections at the lattice truncations. With the present model, the error contributed by the stepped surfaces should be of greater significance because the effect of the imperfect lattice truncation is reduced by the loss of the tissue media.

V. THE HEAT CONDUCTION MODEL

In this section we discuss the assumptions on which the heat conduction model of the microwave-irradiated eye is based. These assumptions involve the mechanism of heat transfer from the eye and the selection of the thermal parameters of the media of the eye. The implementation of these assumptions in the solution of the heat conduction equation is then discussed. Throughout, the tissue geometry and lattice point notation is consistent with that used for the microwave scattering problem.

The basic assumption of the heat conduction model of the irradiated eye is that the chief cooling mechanism is localized at the surface of the eyeball in the form of the retinal blood supply. This is supported by two observa-

tions. First, the interior of the eyeball is largely without blood supply [20]. Second, 70 percent of the overall blood stream supplied to the eye flows through the capillary layer of the choroid, which is adjacent to the retina and mainly responsible for its cooling [23]. This capillary layer extends over much of the surface of the eyeball. Over the remainder, surface cooling is accomplished through the tearing and wiping mechanism of the eyelids. Therefore, in formulating the heat conduction model of the eye, cooling of the eyeball through contact with the fat and muscle tissues of the orbit is ignored. The heat conduction equation is solved only for lattice points within the interior of the eyeball, subject to a boundary condition approximating the cooling of the retinal blood supply and the eyelids.

For simplicity in solving the heat conduction equation, the eye-tissue parameters ρ (density), C_p (specific heat), and K (thermal conductivity) are taken to be independent of position, temperature, and time. Further, these parameters are assumed to be those of water: $\rho = 1000$ kg/m^3, $C_p = 4178$ J/kg·°C, $K = 0.627$ W/m·°C. This assumpton is made because the aqueous and vitreous humors, which comprise the bulk of the eyeball, have a water content of about 99 percent by weight [21].

The partial differential equation of heat conduction that is solved over the volume of the eyeball is

$$\rho C_p \frac{\partial T(\boldsymbol{x},t)}{\partial t} = K\nabla^2 T(\boldsymbol{x},t) + Q(\boldsymbol{x},t) \tag{12a}$$

where T is the unknown temperature function and Q is the heating potential due to microwave irradiation. $Q(\boldsymbol{x},t)$ is related to the incident power level P_{inc} and the computed normalized microwave heating potential Q_n by

$$Q(\boldsymbol{x},t) = E_{\text{inc}}{}^2 \frac{\sigma(\boldsymbol{x}) \mid \boldsymbol{E}(\boldsymbol{x}) \mid^2}{2E_{\text{inc}}{}^2} U(t) = 2\eta_0 P_{\text{inc}} \cdot Q_n(\boldsymbol{x}) \cdot U(t) \tag{12b}$$

where $\eta_0 = (\mu_0/\epsilon_0)^{1/2}$, P_{inc} is given in watts/m^2, and $U(t)$ is the unit step function at $t = 0$. The initial conditions are given by

$$T(\boldsymbol{x},0) = 37°\text{C} \quad \text{(nominal body temperature)}. \tag{12c}$$

The boundary condition at the surface of the eyeball, approximating the cooling of the retinal blood supply, is given by

$$h \cdot (T(\boldsymbol{r},t) - 37) = K \frac{\partial T(\boldsymbol{r},t)}{\partial n} \tag{12d}$$

where $\boldsymbol{r}$ is a point on the eyeball surface, $\boldsymbol{n}$ is the unit vector normal to the surface at $\boldsymbol{r}$, and h is a heat transfer parameter in units of W/m^2·°C. h is assumed constant over the entire surface of the eye and may range in value from zero to infinity. For $h = 0$, $\partial T/\partial n = 0$ at the eye surface and the eye is insulated. For $h = \infty$, $T = 37$°C at the eye surface, the nominal body temperature.

We now estimate a range of values of h that is physically meaningful for this model. The average metabolic rate of body tissues is given as 1 mW/cm^3 [24]. We assume that the heat transfer mechanism of (12d), working over the entire surface of the eyeball, is capable of dealing with this magnitude of heat generation over the volume of the eye. Therefore, h is estimated as

$$h \approx \frac{\text{metabolic rate} \cdot \text{volume of model eyeball}}{(\text{eye surface temperature} - 37°\text{C}) \cdot \text{surface area of model eyeball.}} \tag{13a}$$

On an order-of-magnitude basis, the temperature difference at the interface of the eye media and the retinal blood supply is estimated to be in the range 0.05°C to 0.5°C under normal conditions with no irradiation. With a model eyeball volume of 5.9 cm^3 and a surface area of 24.2 cm^2, h is thus estimated to satisfy the inequality

$$5 \text{ W/m}^2\cdot°\text{C} < h < 50 \text{ W/m}^2\cdot°\text{C}. \tag{13b}$$

During microwave irradiation, h is assumed to remain fixed at its estimated, nominal value.

There is one major simplification implicit in the heat conduction model of (12a)–(12d): the blood-flow network at the eye surface is assumed to have no detailed structure. A more sophisticated model would consider the effects of the location of blood vessels, the velocity and temperature of blood flow, and the variation of blood-flow parameters with temperature. Guy *et al.* [25] have recently developed several elements of the improved model for the rabbit eye. The further elaboration of this method and its application to the human eye is a subject of future work.

The boundary and initial value problem posed by (12a)–(12d) is solved numerically using an IAD algorithm.[2] The lattice points used are those points of the lattice of Fig. 1 that lie within the model eyeball. In this way, a value of the computed microwave heating potential Q_n is available at each lattice point. Symmetry is again used to reduce the storage and execution-time requirements of the program. The even symmetry of the eye geometry and the potential Q_n assures that $T(\boldsymbol{x},t)$ must also possess even symmetry. This can be programmed as

$$T^n(20,j,k) = T^n(19,j,k) \tag{14a}$$

$$T^n(i,j,19\tfrac{1}{2}) = T^n(i,j,18\tfrac{1}{2}). \tag{14b}$$

Boundary condition (12d) may be translated into a form useful for the IAD algorithm. For example, in calculating the intermediate temperature value $T^*(i,j,k)$ along each lattice line parallel to the x axis, we have

$$T^*(i_{\min},j,k) = \frac{37h\delta}{K + h\delta} + \frac{KT^*(i_{\min} + 1,j,k)}{K + h\delta} \tag{15}$$

as the necessary boundary condition at point $(i_{\min},j,k)$. In (15), it is assumed that points $(i_{\min} + 1,j,k)$,

[2] The listing of the 195 card Fortran IV source deck is available from the authors.

$(i_{\min}+2,j,k),\cdots,(19,j,k)$ lie in the interior of the model eyeball, and that the values of T^* at these points are to be obtained with a simultaneous solution. Conditions similar to (15) can be formulated or the T^{**} and T^{n+1} iterations along y- and z-directed lines, respectively.

VI. RESULTS OF THE HEAT CONDUCTION PROGRAMS

In this section, we compare the results of the heat conduction programs for the two frequencies of irradiation of the model eye. The storage and execution time requirements of each program are noted. Next, the computed results are presented as contour maps of the steady-state temperature function at the two symmetry planes of the eyeball. Then the effect of varying parameter h on the approach of the temperature function to the steady state is examined. Last, the significance of the results is discussed.

Each run of the heat conduction program required about 18 000 words of central memory for compilation. All programs were run for 200 time steps, with $\delta t = 4$ s. This proved sufficient to reach the thermal steady state for all cases except for those with h fixed at the minimum value in its range. The execution time required for each run was 88 s.

Fig. 7(a) and (b) gives contour maps of the computed steady-state temperatures at lattice symmetry plane $z = 19\delta$ for incident frequencies of 750 MHz and 1.5 GHz, respectively. Fig. 8(a) and (b) are the corresponding contour maps at lattice symmetry plane $x = 19\frac{1}{2}\delta$. In all

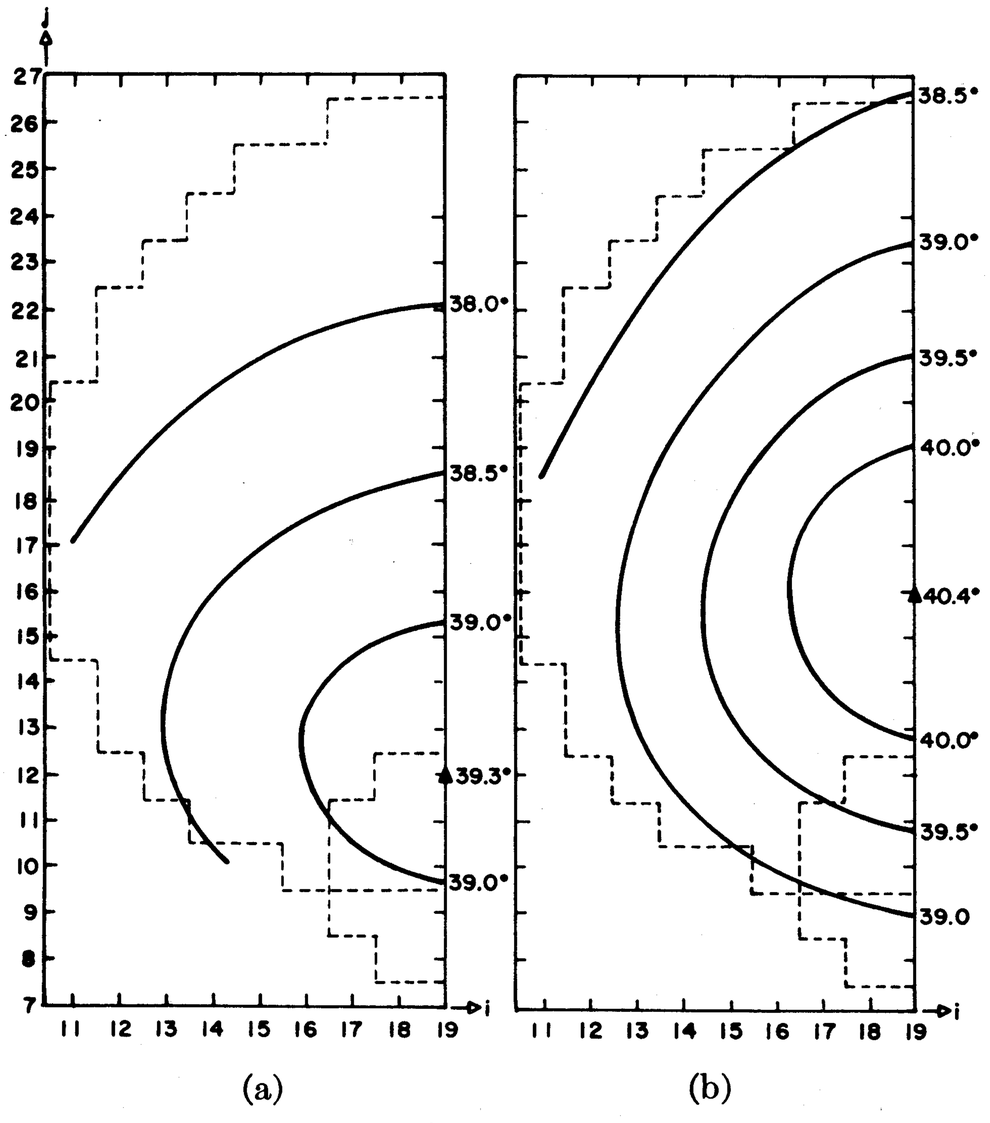

(a) (b)

Fig. 7. Maps of the computed steady-state temperatures at lattice symmetry plane $z = 19\delta$ for $P_{inc} = 100$ mW/cm² and $h = 50$ W/m²·°C. (a) Incident frequency = 750 MHz. (b) Incident frequency = 1.5 GHz.

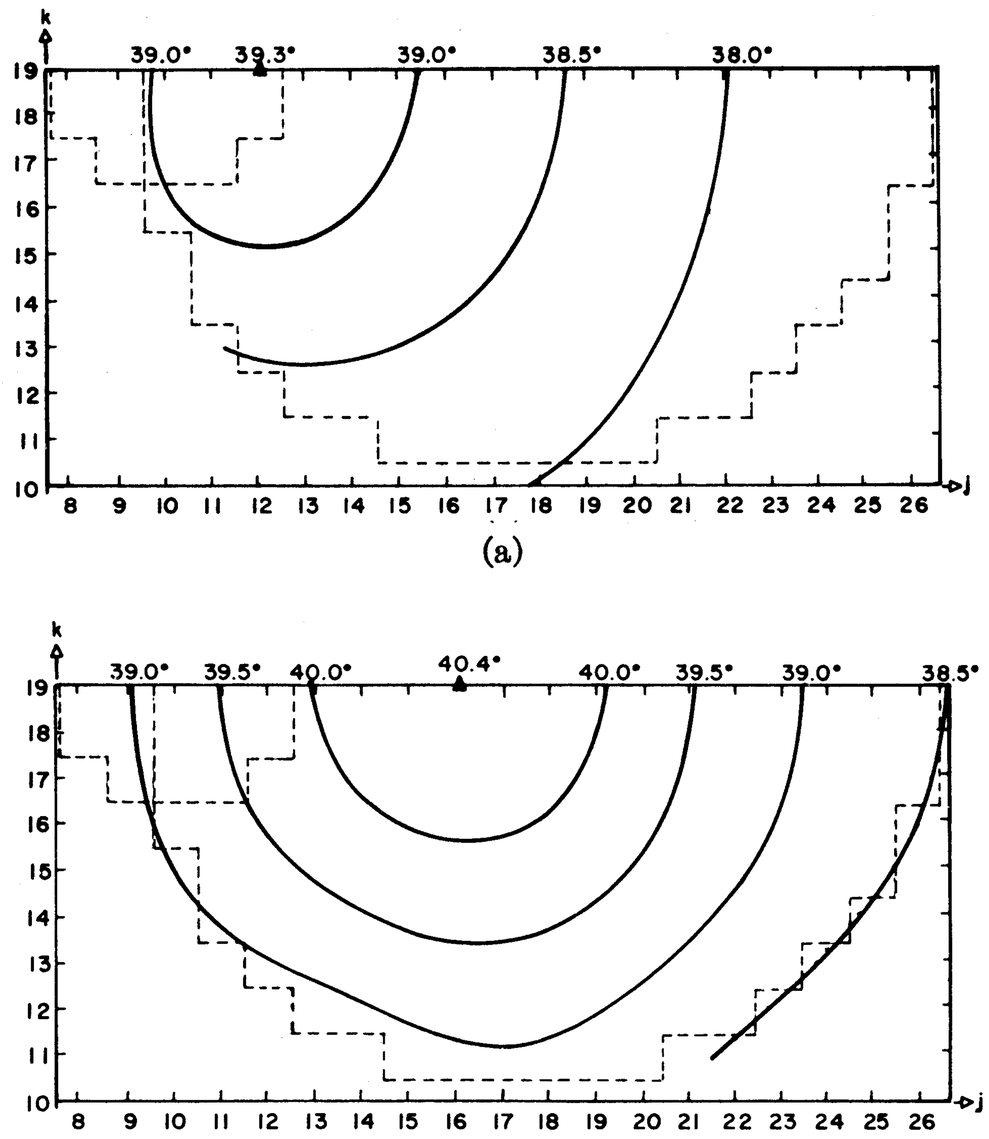

(a)

(b)

Fig. 8. Maps of the computed steady-state temperatures at lattice symmetry plane $x = 19\frac{1}{2}\delta$ for $P_{inc} = 100$ mW/cm² and $h = 50$ W/m²·°C. (a) Incident frequency = 750 MHz. (b) Incident frequency = 1.5 GHz.

of the maps, parameter h is fixed at $50 W/m^2\cdot°C$, and power level P_{inc} is fixed at 100 mW/cm². The dashed lines indicate the boundaries of the tissues of the eyeball.

For the case of 750-MHz irradiation, the peak temperature of 39.3°C is located at the back of the lens. For the 1.5-GHz case, the peak temperature of 40.4°C is located at about the center of the eyeball. We see that the lens temperature due to 1.5-GHz heating is higher than that due to 750-MHz heating, even though the magnitude of the heating potential in the lens area follows an exactly opposite behavior. Evidently, this is because the surface cooling mechanism of the model eye is more effective for the shallow 750-MHz heating pattern than for the relatively deep 1.5-GHz heating pattern. This is a strong indication that tissue thermodynamics must be taken into account when analyzing microwave heating of organs.

Fig. 9 is a graph of the peak eye temperature versus time, for the 1.5-GHz case. The two curves plotted represent the behavior of this temperature for the extreme values of the range of h of (13b). Irradiation is assumed to begin at $t = 0$ and continue from then on with a constant power level of 100 mW/cm². We see that for $h = 50$ W/m²·°C thermal equilibrium is reached about 10 min after the start of heating, with a maximum temperature of about 40.4°C. However, for $h = 5$ W/m²·°C, equilibrium is not attained until much later, estimated to be about 45 min. For this case, the maximum achieved temperature is about 56°C. This implies that the peak

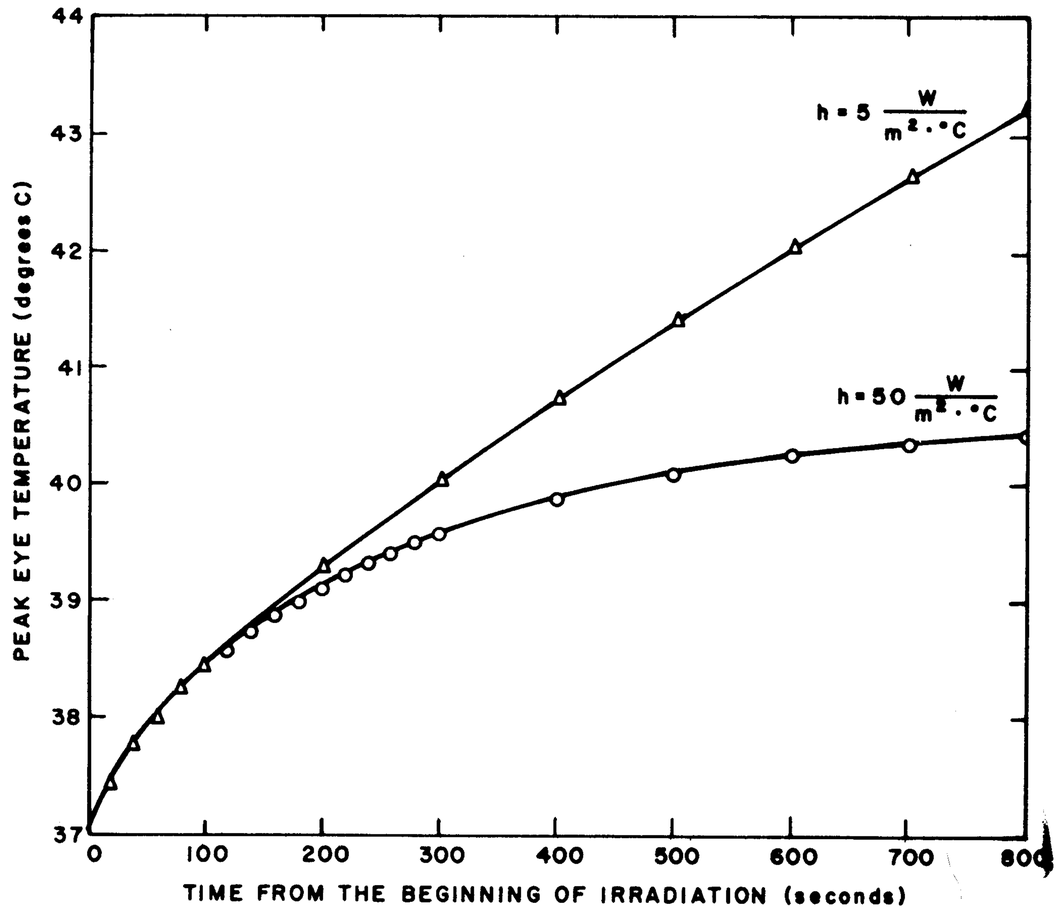

Fig. 9. Range of the peak eye temperature versus time for incident frequency = 1.5 GHz and P_{inc} = 100 mW/cm².

temperature within the model eye is in the range of 40.4°C to 56°C for the assumed range of values of h.

For comparison with the results presented here, we note the temperature distribution within the rabbit eye irradiated at 2.45 GHz, computed by Guy *et al.* [25]. For P_{inc} = 100 mW/cm², a maximum temperature of 40.0°C was calculated on the center line of the eyeball, approximately $\frac{2}{3}$ of the eyeball diameter from the front surface. Thermal equilibrium was reached within about 20 min of the start of irradiation. The magnitude and position of the peak rabbit-eye temperature and the time required to reach the steady state agree well with the 1.5-GHz results (with h = 50 W/m²·°C) for the human-eye model reported in this paper. This agreement offers promise that a relation between the microwave heating of the rabbit eye and of the human eye can be established.

VII. CONCLUSIONS

The absorbed power distribution pattern within a detailed model of the microwave-irradiated human eye has been computed for two different frequencies of plane-wave irradiation, 750 MHz and 1.5 GHz. The temperature distribution induced by the microwave heating within the model eye has been computed. The results indicate that a distinct hot spot exceeding 40.4°C probably occurs deep within the eye at a frequency of 1.5 GHz. The results imply that hot spots within the eye are to be expected at frequencies higher than 1.5 GHz, due to wave-concentration effects of the eyeball–orbit juxtaposition. Comparison of the temperatures within the human-eye model with those calculated by Guy *et al.* [25] for the rabbit eye indicates the possibility of relating the microwave heating patterns within the respective organs. A more detailed model of the human eye and computer runs for frequencies higher than 1.5 GHz are required to explore this possible relation.

REFERENCES

[1] F. G. Hirsch and J. T. Parker, "Bilateral lenticular opacities occurring in a technician operating a microwave generator," *Am. Med. Assoc. Arch. Ind. Hyg.*, vol. 6, pp. 512–517, Dec. 1952.
[2] M. M. Zaret, "An experimental study of the cataractogenic effects of microwave radiation," Zaret Foundation Rep. RADC-TDR-64-273 (Contract AF 30(602)-3087), Oct. 1964.
[3] L. Birenbaum, G. M. Grosof, S. W. Rosenthal, and M. M. Zaret, "Effect of microwaves on the eye," *IEEE Trans. Biomed. Eng.*, vol. BME-16, pp. 7–14, Jan. 1969.
[4] R. L. Carpenter, D. K. Biddle, and C. A. Van Ummersen, "Opacities in the lens of the eye experimentally induced by exposure to microwave radiation," *IRE Trans. Med. Electron.*, vol. PGME-7, pp. 152–157, July 1960.
[5] S. M. Michaelson, "Biological effects of microwave exposure," in *Proc. Biological Effects and Health Implications of Microwave Radiation Symp.*, Med. College Virginia (Richmond, Sept. 1969), Rep. BRH/DBE 70-2, Sept. 1969, pp. 35–58.
[6] *U. S. A. Standard*, "Safety level of electromagnetic radiation with respect to personnel," U.S.A. Standards Inst., New York, N. Y., USAS C95.1, 1966.
[7] A. W. Guy, "Future research directions and needs in biologic electromagnetic radiation research," in *Biologic Effects of Nonionizing Radiation, Ann. N. Y. Acad. Sci.*, vol. 247, pp. 539–545, Feb. 1975.
[8] A. W. Guy, J. C. Lin, P. Kramar, and A. F. Emery, "Measurement of absorbed power patterns in the head and eyes of rabbits exposed to typical microwave sources," in *Proc. 1974 Conf. Precision Electromagnetic Measurements* (London, England, July, 1974), pp. 255–257.
[9] A. Anne, M. Saito, O. M. Salati, and H. P. Schwan, "Penetration and thermal dissipation of microwaves in tissues," Univ. Pennsylvania, Philadelphia, Tech. Rep. RADC-TDR-62-244, Contract AF30(602)-2344, ASTIA Doc. 284 981, 1962.
[10] H. F. Cook, "A physical investigation of heat production in human tissues when exposed to microwaves," *Brit. J. Appl. Phys.*, vol. 3, pp. 1–6, 1952.
[11] A. R. Shapiro, R. F. Lutomirski, and H. T. Yura, "Induced fields and heating within a cranial structure irradiated by an electromagnetic plane wave," *IEEE Trans. Microwave Theory Tech.* (*Special Issue on Biological Effects of Microwaves*), vol. MTT-19, pp. 187–196, Feb. 1971.
[12] J. A. Stratton, *Electromagnetic Theory*. New York: McGraw-Hill, 1941, pp. 563–573.
[13] D. E. Livesay and K.-M. Chen, "Electromagnetic fields induced inside arbitrarily shaped biological bodies," *IEEE Trans. Microwave Theory Tech.* (*Part II of Two Parts—1974 Symp. Issue*), vol. MTT-22, pp. 1273–1280, Dec. 1974.
[14] T. K. Wu and L. L. Tsai, "Numerical analysis of electromagnetic fields in biological tissues," *Proc. IEEE* (Lett.), vol. 62, pp. 1167–1168, Aug. 1974.
[15] B. H. McDonald and A. Wexler, "Finite-element solution of unbounded field problems," *IEEE Trans. Microwave Theory Tech.* (*1972 Symp. Issue*), vol. MTT-20, pp. 841–847, Dec. 1972.
[16] D. R. Wilton and R. Mittra, "A new numerical approach to the calculation of electromagnetic scattering properties of two-dimensional bodies of arbitrary cross section," *IEEE Trans. Antennas Propagat.*, vol. AP-20, pp. 310–317, May 1972.
[17] A. Taflove and M. E. Brodwin, "Numerical solution of steady-state electromagnetic scattering problems using the time-dependent Maxwell's equations," *IEEE Trans. Microwave Theory Tech.*, vol. MTT-23, pp. 623–630, Aug. 1975.
[18] B. Carnahan, H. A. Luther, and J. O. Wilkes, *Applied Numerical Methods*. New York: Wiley, 1969, pp. 452–461.
[19] P. L. Brian, "A finite-difference method of high-order accuracy for the solution of three-dimensional transient heat conduction problems," *Amer. Inst. Chem. Eng. J.*, vol. 7, pp. 367–370, 1961.
[20] S. Duke-Elder and K. C. Wybar, *System of Ophthalmology. Vol. II: The Anatomy of the Visual System*. London, England: Kimpton, 1961, ch. 5.
[21] H. Davson, Ed., *The Eye. Vol. 1: Vegetative Physiology and Biochemistry*. New York: Academic, 1962.
[22] C. C. Johnson and A. W. Guy, "Nonionizing electromagnetic wave effects in biological materials and systems," *Proc. IEEE*, vol. 60, pp. 692–718, June 1972.
[23] A. Roulier, "Calculation of temperature increase in the eye produced by intense light," *Bull. Math. Biophys.*, vol. 32, pp. 403–427, 1970.
[24] H. P. Schwan, "Microwave radiation: biophysical considerations and standards criteria," *IEEE Trans. Biomed. Eng.*, vol. BME-19, pp. 304–312, July 1972.
[25] A. W. Guy, J. C. Lin, P. O. Kramar, and A. F. Emery, "Effect of 2450-MHz radiation on the rabbit eye," *IEEE Trans. Microwave Theory Tech.*, vol. MTT-23, pp. 492–498, June 1975.